THE JOURNAL OF PHYSICAL CHEMISTRY C

Article

Cite This: J. Phys. Chem. C 2019, 123, 29986−29993

pubs.acs.org/JPCC

Oxidized Silicon Sulfide: Stability and Electronic Properties of a Novel Two-Dimensional Material

Zhengnan Li, Shixin Song, Shuai Dong, and Jie Guan*

School of Physics, Southeast University, Nanjing 211189, PRC

Supporting Information

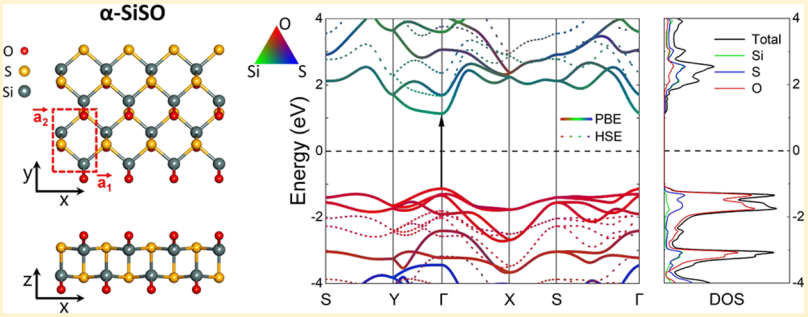

ABSTRACT: The monolayer form of oxidized silicon sulfide (SiSO) structures are predicted and the stability and electronic properties are investigated by ab initio density functional calculations. The most stable configurations of isolated oxygen impurities for four different two-dimensional (2D) SiS structures are determined and all the the calculated binding energies were found to be larger than those for phosphorene, due to the lower electronegativity of Si atoms. Four 2D stoichiometric SiSO structures corresponding to the most stable oxidation configurations are predicted and 2D α-SiSO is demonstrated to be stable by phonon spectra calculations and ab initio molecular dynamics simulations. Electronic structure calculations indicate that α-SiSO monolayer is semiconducting with a direct band gap, which can be effectively tuned by uniaxial in-layer strain. The value of band gap and thermodynamic stability are found depending sensitively on the degree of oxidation.

1. INTRODUCTION

There is a dramatically growing interest in two-dimensional (2D) materials as monolayer graphene was exfoliated successfully.[1] Phosphorene, a monolayer of black phosphorus, has attracted significant attention since 2014 due to its semiconducting character and high carrier mobility.[2−5] As the isoelectric counterpart of phosphorene, monolayer silicon monosulfide (SiS) has been predicted shortly afterward[6,7] and the group-IV monochalcogenide family (GeSe, SnSe, SnTe, ...) have become an important group of the 2D materials with their interesting novel properties.[8−24] The potential applications of 2D group-IV monochalcogenides in low-dimensional piezoelectrics,[10,11] ferroelectrics,[13−16] thermoelectrics,[17,18] electrochemics,[19] and optoelectronics[20−24] have been well explored in both theory and experiment.

The chemical reactivity in air, which is a significant problem in phosphorene,[25−28] could also be a challenge in the application of 2D group-IV monochalcogenides, as a result of their similarity in structure. Point oxygen defects in SnS, SnSe, GeS, and GeSe monolayers have been studied theoretically and shown that these materials are less prone to oxidation than phosphorene.[29] However, 2D SiS, consisting of lighter elements, can be much easier to be oxidized due to the smaller atomic radii and stronger chemical bonding to oxygen. The inclination to oxidize could be the main impediment to the experimental realization of 2D SiS structures. On the other hand, oxidation could be an effective way of chemical modification for 2D materials to tailor their physical and electrical properties.[30−34] In particular, oxidized phosphorene have been shown to be stable in the monolayer form and the electronic properties can be effectively tuned by the controlled oxidation level.[35,36] The 2D form of the oxidized SiS structures, by analogy to phosphorene oxide, is also expected to exist and has much different chemical and electronic properties from pristine SiS. However, to the best of the authors' knowledge, neither the oxygen defects nor the uniformly oxidized SiS structures have been explored so far.

In this study, to fill the missing information for the oxidation of SiS, four stable pristine 2D SiS structures are considered. According to our ab initio density functional calculations, binding energies for the most stable configurations of oxygen impurities in all the four 2D SiS structures are larger than that in phosphorene, which indicates the inclination to oxidation, due to the lower electronegativity of Si atoms. Four 2D stoichiometric SiSO structures corresponding to the most stable oxidation configurations are predicted. α-SiSO, among the four SiSO structures, is demonstrated to be the most stable by phonon spectra calculations. Electronic structure calcu-

Received: August 22, 2019
Revised: November 12, 2019
Published: November 14, 2019

DOI: 10.1021/acs.jpcc.9b08025
J. Phys. Chem. C 2019, 123, 29986−29993

lations indicate that α-SiSO is semiconducting with a direct band gap, which can be effectively tuned by uniaxial in-layer strain. Finally, non-stoichiometric α-$SiSO_x$ ($x < 1$) structures with partial oxidation are studied. We found that the value of band gap and thermodynamic stability, which is determined by our ab initio molecular dynamics (AIMD) simulations, depend sensitively on the degree of oxidation.

2. THEORETICAL METHODS

We utilized ab initio density functional theory (DFT) as implemented in the VASP code[37−39] to obtain insights into the equilibrium structure, stability, electronic properties, and AIMD simulations of SiS and corresponding oxidized structures reported here. Periodic boundary conditions are used throughout the study, with 2D structures represented by a periodic array of slabs separated by a vacuum region in excess of 15 Å. The reciprocal space is sampled by a fine grid[40] of dimension 8 × 8 × 1 k-points in the Brillouin zone of the unit cell with 16 atoms or its equivalent in other supercells. We used projector-augmented-wave pseudopotentials[41] and the Perdew−Burke−Ernzerhof (PBE)[42] exchange−correlation functionals. Electronic wave function is expanded on a plane-wave basis set with a cutoff energy of 500 eV. A total energy difference of below 10^{-5} eV between subsequent self-consistency iterations is used as the criterion for reaching self-consistency. All geometries have been optimized using the conjugate-gradient method,[43] until none of the residual Hellmann−Feynman forces exceeded 10^{-2} eV/Å. The phonon calculations are carried out using the supercell approach, as implemented in the PHONOPY code.[44] In the AIMD simulations, supercells including more than 100 atoms are used and the temperatures of 300 and 500 K are kept for longer than 6 ps with a time step of 3 fs. The hybrid HSE06 functional[45] and GW method[46,47] were used to obtain more accurate band structures and the value of band gaps. van der Waals (vdW) correction was included in the multilayer systems using the DFT-D2[48] method.

3. RESULTS AND DISCUSSION

3.1. Isolated Oxygen Impurities. Four different 2D SiS structures predicted in previous works were considered, that is α-SiS, β-SiS[6] and *Pma*2-SiS, silicene sulfide.[7] As per the optimized structures for the monolayers shown in the first row of Figure 1, α-SiS and β-SiS are isoelectronic with black and blue phosphorene,[49,50] respectively. Therefore, they are similar to phosphorene in geometry with all atoms threefold coordinated. However, in *Pma*2-SiS and silicene sulfide, all the atoms obey the "octet rule" with Si fourfold coordinated and S twofold coordinated. α-SiS and *Pma*2-SiS have orthorhombic lattices, β-SiS has a honeycomb lattice and silicene sulfide has a stretched honeycomb lattice with the angle of 63.88° between lattice vectors. All the calculated structural characteristics are summarized in Table 1 and consistent with those reported in previous works.[6,7]

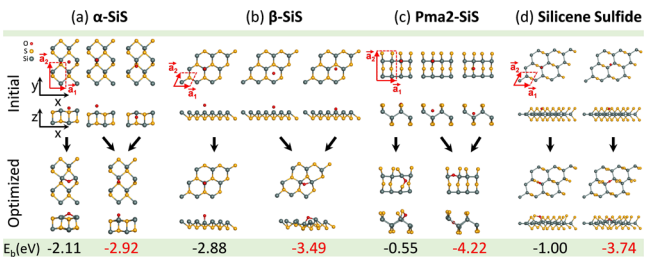

Figure 1. Possible configurations of isolated oxygen atom absorbed on the monolayer of (a) α-SiS, (b) β-SiS, (c) *Pma*2-SiS, (d) silicene sulfide. Ball-and-stick model in the top view and side view of initial structures are shown in the first row and that of optimized structures in the second row. Lattice vectors are indicated by red arrows in the top view of the initial structures. Calculated binding energies E_b are given at the bottom and those for the most stable configurations are highlighted in red.

Table 1. Calculated Structural Characters of Pre-oxidized and Post-oxidized SiS Structures[a]

	$\lvert\vec{a_1}\rvert$ (Å)	$\lvert\vec{a_2}\rvert$ (Å)	$\angle\vec{a_1}\vec{a_2}$ (deg)
α-SiS	3.31	4.38	90
β-SiS	3.30	3.30	60
*Pma*2-SiS	3.98	6.64	90
silicene sulfide	4.56	4.01	63.88
α-SiSO	3.41	4.75	90
β-SiSO	2.87	3.33	64.47
*Pma*2-SiSO	5.23	6.63	90
silicene sulfide-O	5.21	4.95	61.63

[a] $\lvert\vec{a_1}\rvert$ and $\lvert\vec{a_2}\rvert$ are the in-plane lattice constants defined in Figures 1 and 2. $\angle\vec{a_1}\vec{a_2}$ is the angle between lattice vectors.

To investigate the resistance to oxidation, interactions between isolated oxygen atoms with all the selected SiS structures were calculated. As shown in Figure 1a, initially three possible configurations for the O atoms approaching α-SiS are considered: the ring site which is above the center of the hexagonal ring, the Si-top site which is on top of the Si atom, and the interstitial site which is close to the Si−S bond and interred into the layer. Interestingly, both the Si-top and interstitial sites prefer the dangling site attaching to the Si atoms in the optimized configurations. The initial ring site was optimized to a Si−O−Si bridge site. To further investigate the energetic stability of the oxygen impurities, the binding energy per oxygen atom is defined as: $E_b = E_{SiS+O} - (E_{SiS} + E_{O_2}/2)$, where E_{SiS+O} is the total energy of a super cell including one O atom in the oxidized SiS layer, E_{SiS} is the total energy of the corresponding super cell in the pristine SiS layer, and E_{O_2} is the total energy of an O_2 molecule. According to the definition, a negative E_b indicates that the oxygen impurity formation is energetically favorable (exothermic reaction). In the equilibrium geometry of oxygen impurities, the binding energy per oxygen atom E_b is −2.92 eV for the Si-dangling site and −2.11 eV for the Si−O−Si bridge site.

Similarly, possible configurations of oxygen impurities in the other three structures are shown in Figure 1b−d. In β-SiS, initially the Si-top site, ring site and Si−O−Si bridge site configurations were considered and the equilibrium configurations of Si-top site with E_b equaling −2.88 eV and Si−O−Si bridge site with E_b equaling −3.49 eV were obtained. In *Pma*2-SiS, initial configurations with O atom embedded in the hollows of S−Si−S, Si−Si−Si, and Si−S−Si bonds were optimized, respectively, and equilibrium configurations of Si−O−S bridge site with E_b equaling −0.55 eV and Si−O−Si bridge site with E_b equaling −4.22 eV were obtained. In silicene sulfide, initial configurations of Si-top site and Si−O−Si bridge site were optimized and equilibrium configurations of

DOI: 10.1021/acs.jpcc.9b08025
J. Phys. Chem. C 2019, 123, 29986−29993

Si−O−S bridge site with E_b equaling −1.00 eV and Si−O−Si bridge site with E_b equaling −3.74 eV were obtained. From all these results, we found that (i) in all the structures the oxygen atom prefer Si atoms to S atoms due to the lower electronegativity of Si, (ii) the most stable configuration of oxygen impurity is Si-dangling site in α-SiS and is Si−O−Si bridge site in the rest, and (iii) binding energies of the most stable oxygen impurities for all the 2D SiS structures are much larger in absolute value than that for other 2D group-IV monochalcogenides, such as SnS (−0.88 eV), SnSe (−0.75 eV), GeS (−1.47 eV), GeSe (−1.22 eV),[29] and also larger than that for phosphorene (−2.08 eV).[27] The large negative binding energy indicates the inclination to oxidize in the air for the selected 2D SiS structures.

3.2. Stoichiometric SiSO Structures. Here we chose the most stable configuration of oxygen impurities in each SiS structure and further studied their corresponding 2D stoichiometric SiSO structures with uniform oxidation. The optimized geometry of α-SiSO monolayer is shown in Figure 2a. Each Si atom is attached by one O atom and the binding energy per oxygen atom E_b equaling −2.70 eV is obtained, which is a little smaller than the value of −2.92 eV for isolated oxygen impurity. This is because of the repulsive interaction between neighboring O atoms in the fully oxidized structure, with details discussed in the Supporting Information. In β-SiSO, neighboring Si atoms are connected by O atoms with E_b equaling −3.48 eV, which is almost the same as isolated bridge-site oxygen impurity, as shown in Figure 2b. *Pma*2-SiSO and silicene sulfide-O structures are similar, where all the pristine Si−Si bonds are broken and new Si−O−Si bonds are formed, instead. Both of them get larger values of E_b (−4.25 eV) than those for isolated oxygen impurities due to the vanishing of distortion in the uniformly oxidized structures. Cohesive energies with respect to isolated atoms for all the four structures have also been calculated and 4.47 eV/atom for α-SiSO, 4.74 eV/atom for β-SiSO, 5.24 eV/atom for *Pma*2-SiSO, and 5.23 eV/atom for silicene sulfide-O have been obtained. Structural characteristics for all the SiSO structures are summarized in Table 1. We found that after oxidation the unit cell of α-SiSO become larger than before. The main reason for this is that the extra Si−O bonds have modified the hybridization of orbitals in Si, enlarged the angles between the three Si−S bonds around each Si atom and finally extended the area of the unit cell in $x - y$ plane. The unit cell of β-SiSO shrinks in x-direction due to the extra Si−O−Si bonding. Both *Pma*2-SiSO and silicene sulfide-O get larger unit cells as a result of O atoms embedding into the lattices.

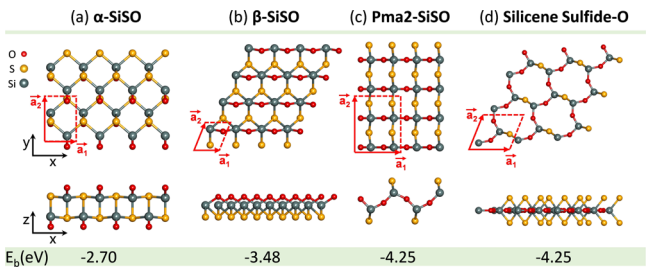

Figure 2. Ball-and-stick model in the top view (1st row) and side view (2nd row) of equilibrium structures for monolayers of (a) α-SiSO, (b) β-SiSO, (c) *Pma*2-SiSO, and (d) silicene sulfide-O. Lattice vectors are indicated by red arrows in the top view. Calculated binding energies E_b are given at the bottom.

As a robust way to illustrate the structural stability, vibrational phonon spectra calculations were carried out for the four equilibrium SiSO structures shown in Figure 2. The results of phonon dispersion based on PBE functional for the monolayers are shown in Figure 3. We found that dynamically the most stable structure is α-SiSO, with essentially no imaginary modes. The tiny U-shaped feature near Γ-point in the out-of-plane acoustic (ZA) mode is caused by the artifact of the method but has nothing to do with a structural instability, which is quite common in other 2D systems.[51,52] In contrast, significant negative frequencies were found in the phonon dispersion of β-SiSO, *Pma*2-SiSO, and silicene sulfide-O, which indicates the dynamic instability of freestanding monolayers. The phonon dispersion based on LDA functional was calculated to further confirm the dynamic stability. As the results shown in Figure S6, α-SiSO is still the most stable one. Structures with dynamically unstable monolayers may still exist in a multilayer form or on a substrate. Thus the electronic band structure for β-SiSO, *Pma*2-SiSO, and silicene sulfide-O monolayers has also been investigated and the results are shown in Figure S7. All the three structures show an indirect gap. Based on our PBE calculations, β-SiSO has a narrow gap of 0.58 eV, while *Pma*2-SiSO and silicene sulfide-O have much larger gaps of 3.71 and 4.50 eV, respectively. α-SiSO structure with the best dynamic stability as shown here will be focused on in the following discussions.

3.3. Electronic Properties of α-SiSO. As a previously unexplored 2D material, the electronic properties of α-SiSO were investigated. The electronic band structure and the associated projected density of states (PDOS) are shown in Figure 4a,b. Our DFT-PBE calculations show that α-SiSO monolayer is a semiconductor with a direct band gap of 2.28 eV. Both the valence band maximum (VBM) and the conduction band minimum (CBM) are located at Γ-point. As the fundamental band gap is usually underestimated by PBE calculations, we have also performed HSE06 calculations with a hybrid exchange−correlation functional of the band structure. As shown by the dashed lines in Figure 4a, the

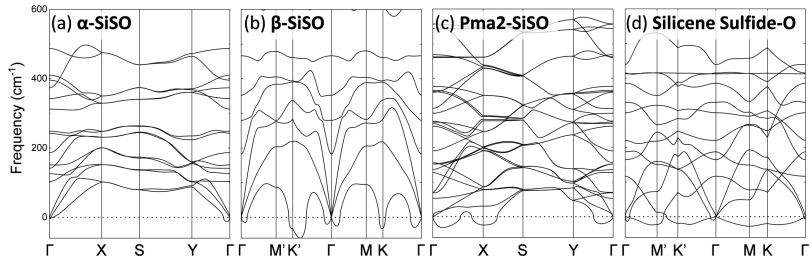

Figure 3. Vibrational phonon spectra for monolayers of (a) α-SiSO, (b) β-SiSO, (c)*Pma*2-SiSO, and (d) silicene sulfide-O.

DOI: 10.1021/acs.jpcc.9b08025
J. Phys. Chem. C 2019, 123, 29986−29993

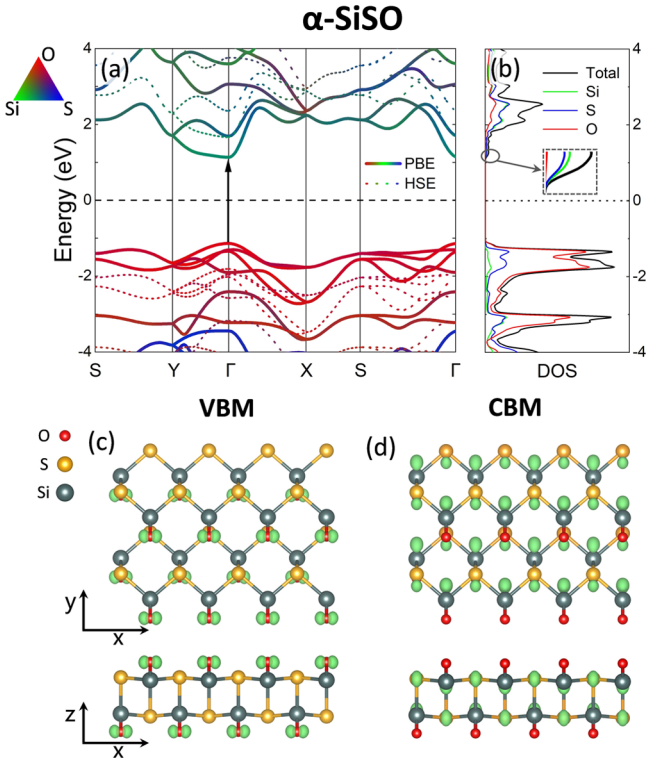

Figure 4. (a) Electronic band structure, (b) PDOS, partial charge density associated with frontier states in the (c) valence band and (d) conduction band of α-SiSO monolayer. Band structures based on both PBE (solid lines) and HSE06 (dashed lines) functionals are shown in (a) and all the results shown in (b–d) are based on PBE functional. Contributions of electrons from different atoms in (a,b) are distinguished by color. A direct band gap is shown by a black arrow in (a). A figure zoomed in near the CBM is shown as inset in (b).

HSE06 dispersion of individual bands closely resemble the PBE results and the only difference is that HSE06 gives a larger band gap of 3.73 eV. Contributions of electrons from different atoms are indicated by different colors in the band structure and PDOS plots. PDOS near the CBM is easier to see from the amplified figure in the inset of Figure 4b. We found that the VBM is dominated by electrons from O, while the CBM is dominated by electrons from Si and S. Computationally more demanding GW method has also been used for the band structure calculation of α-SiSO. As the comparison of GW, HSE06 and PBE results shown in Figure S8, the three methods almost give the same band dispersion for both valence bands and conduction bands while GW method gives a much larger band gap of 5.28 eV, which may be significantly overestimated.[53] Computationally less-involved PBE and HSE06 methods are used in our following further discussions.

More details about the electron characters of the VBM and CBM were explored by partial charge density plotting associated with frontier states, as depicted in Figure 4c,d. The charge distribution in the VBM was found surrounding O atoms and appears a dumbbell-like shape along x-direction, which is a signature of the domination of p_x orbitals from oxygen. The charge distribution in the CBM is much different and appears a polarized s orbitals along y-direction surrounding Si and S atoms, which is the signature of a hybridization of s and p_y orbitals from Si and S. The results can be further verified by detailed PDOS plotting for different orbitals from each single element shown in Supporting Information. We also found from Figure 4a that the band dispersion is much flatter along $\Gamma - Y$ direction than that along $\Gamma - X$ direction near the CBM at Γ-point, which indicates a significant anisotropic carrier effective mass. This can be understood because the frontier states at the CBM from Si and S are very close to each other and can have a strong interaction along x-direction, as shown in Figure 4d.

Similar to other nonplanar 2D systems like phosphorene and SiS, α-SiSO is susceptible to even minute in-plane strain. To quantify the effect, the overall dependence of the stability and the fundamental band gap on the tensile and compressive in-layer strain of α-SiSO was calculated and the results are presented in Figure 5. We have considered uniaxial strain along

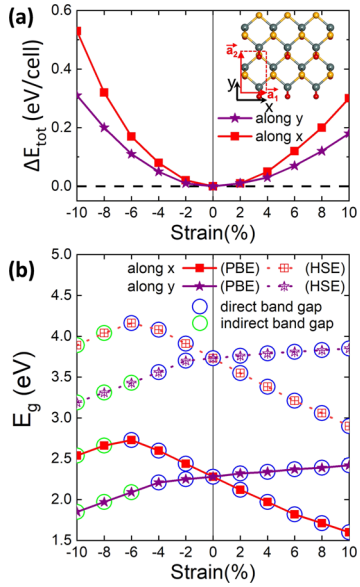

Figure 5. Effect of uniaxial in-layer strain on (a) the relative total energy ΔE_{tot} and (b) the fundamental band gap E_g in α-SiSO monolayer. The strain directions defined in the inset of (a) are distinguished by color and symbols. The values of band gaps based on PBE and HSE06 functionals are shown by solid and dashed lines, respectively, in (b). Direct and indirect band gaps are marked by blue and green circles, respectively, in (b).

x- and y-direction, as defined in the inset of Figure 5a. A distinct anisotropy of the strain energy with respect to the strain direction is shown in Figure 5a, which results from the distinct structural anisotropy. Similar to other phosphorene-like buckled structures, the system appears softer when strained along the armchair-like direction (y-direction) than the other one. We found that the overall strain energy ΔE_{tot} is quite small, which is about 0.53 or 0.30 eV/cell under 10% compressive or tensile strain, respectively, along x-direction. The value for strain along the softer y-direction is almost halved, which is about 0.30 or 0.18 eV/cell under 10% compression or stretch, respectively. The small strain energy indicates a good flexibility under in-layer strain for α-SiSO monolayer. Elastic constants of α-SiSO were further calculated by the approach previously reported for 2D systems.[54] The obtained elastic stiffness constants C_{11} of 130 GPa, C_{22} of 82 GPa, C_{12} of 33 GPa, and C_{66} of 25 GPa confirm the anisotropic elasticity and good in-layer flexibility.

The effect of uniaxial in-layer strain on the fundamental band gap obtained by our PBE and HSE06 calculations is

DOI: 10.1021/acs.jpcc.9b08025
J. Phys. Chem. C 2019, 123, 29986–29993

shown in Figure 5b. From the PBE results shown by the solid lines we found that the band gap reduces down to 1.60 eV under the $\lesssim$10% stretch along x-direction. When compressed, the band gap increases and reach the largest value of 2.73 eV under 6% compression. When the compressive strain exceeds 6%, the value of band gap will decrease and in the meantime the direct gap is transformed to an indirect gap, as marked by the green circles. A generally opposite effect was found along y-direction with the value of the band gap varying between 1.85 eV under 10% compressive strain and 2.42 eV under 10% tensile strain. A direct-to-indirect gap transition was also found by a $\gtrsim$4% compression along y-direction. The HSE06 calculations give almost the same trend as PBE, except for a rigid upshift of about 1.4 eV for the gap values of all the strained structures, as shown by the dashed lines in Figure 5b. The detailed band structures for all the strained structures discussed here are depicted in Supporting Information.

Interlayer interaction and the electronic properties have also been investigated in the multilayer and bulk systems of α-SiSO. Our DFT results show that AA stacking multilayer and bulk systems of α-SiSO are preferred, as the structural model shown in Figure S5a. Interlayer binding energy (ΔE) and the PBE band gap as a function of the number of layer are depicted in Figure S5b,c. It shows that ΔE is 0.03 eV/atom for the bilayer and 0.06 eV/atom for the bulk of α-SiSO. This is a typical vdW interlayer interaction and a little weaker than that of black phosphorus, which is about 0.04 eV/atom for the bilayer and 0.08 eV/atom for the bulk.[55] What is different from traditional 2D materials such as phosphorene is that generally the value of band gap slightly increases as the number of layer increases, from 2.28 eV for the monolayer to 2.35 eV for the bulk.

3.4. Effects of Oxidation Degree. Effects of the oxidation degree on 2D α-SiSO were examined by the calculations for α-$SiSO_x$ ($0 < x < 1$) structures. Monolayers of α_1-$SiSO_{0.5}$, α_2-$SiSO_{0.5}$, and α-$SiSO_{0.25}$ were optimized and the equilibrium geometries are depicted in Figure 6a–c. In α_1-$SiSO_{0.5}$, O atoms are attached to Si atoms on only one single side of α-SiS while in α_2-$SiSO_{0.5}$ O atoms are attached on both sides with the density halved. Finally, in α-$SiSO_{0.25}$ O atoms are only attached to half of the Si atoms on one single side. Our PBE and HSE06 results for electronic band gaps of the selected α-$SiSO_x$ ($0 \le x \le 1$) monolayers are summarized in Figure 6d. Interestingly, we found that the value of the band gap increases with the value of x if oxidation happens on both sides of the monolayer, from 1.43 eV (2.31 eV) for α-SiS to 2.28 eV (3.73 eV) for α-SiSO based on PBE (HSE06) calculations. However, if oxidation happens on a single side, the results are much different. The value of band gap decreases slightly when x increases (from 1.43 eV for α-SiS to 1.25 eV for α_1-$SiSO_{0.5}$) in PBE and almost keeps unchanged at about 2.32 eV as x increases in HSE06. The detailed band structure and PDOS plots for α-$SiSO_x$ ($0 < x < 1$) are shown in Supporting Information. This finding provides another way to effectively tune the electronic properties of the pristine 2D structure by appropriate oxidation.

Besides the electronic properties, the effect of oxidation degree on the thermodynamic stability for 2D α-$SiSO_x$ ($0 \le x \le 1$) structures were investigated by AIMD simulations. Our canonical MD simulations for monolayers of α-SiS, α-SiSO, α_1-$SiSO_{0.5}$, α_2-$SiSO_{0.5}$ and α-$SiSO_{0.25}$ were performed under the temperature 300 and 500 K, respectively. We found that α-SiS, α-SiSO and α_1-$SiSO_{0.5}$ are stable under both 300 and 500 K. As the results under 300 and 500 K are similar, here we present

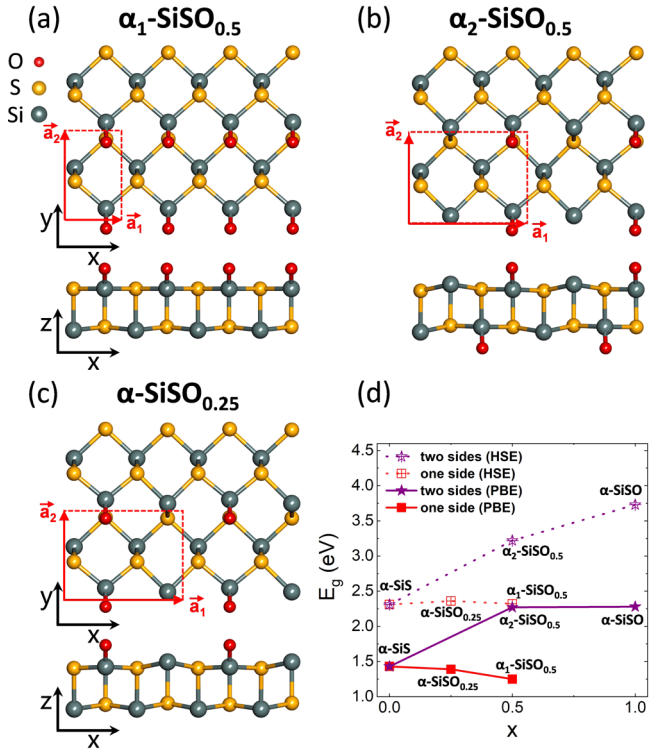

Figure 6. Ball-and-stick model in the top view and side view of equilibrium structures for (a) α_1-$SiSO_{0.5}$, (b) α_2-$SiSO_{0.5}$, and (c) α-$SiSO_{0.25}$. Lattice vectors are indicated by red arrows in the top view. (d) The value of band gap E_g as a function of x for α-$SiSO_x$ monolayers. Structures with oxidation on one single side and both sides are distinguished by color and symbols. Results based on PBE and HSE06 functionals are shown by solid and dashed lines, respectively.

the snapshots and the fluctuations of total potential energy during the MD process under 500 K in Figure 7a–c. We can see that all the three structures keep their geometries nearly unchanged during a simulation time up to 6 ps, which indicates good thermodynamic stabilities at high temperature. However, the other two structures are not stable under either 300 or 500 K. The snapshots and energy fluctuations during the MD process under 300 K for α_2-$SiSO_{0.5}$ and α-$SiSO_{0.25}$ are shown in Figure 7d,e. We can see that α_2-$SiSO_{0.5}$ gets significantly distorted and finally degraded after 1.5 ps. The reason for this is that in α_2-$SiSO_{0.5}$, each oxidized surface is not saturated with bare Si atoms. The O atom attached to one Si is easily attracted by the neighboring exposed Si atoms and forms a bridge configuration. This will cause a significant distortion of the global structure and finally break the structure. The situation is much different in α-SiSO and α_1-$SiSO_{0.5}$ because there are no bare Si atoms on each oxidized surface. Each O atom is restricted bonding to one Si and cannot move away due to the repulsive interaction from the neighboring O atoms, which was mentioned above and also in Supporting Information. In α-$SiSO_{0.25}$, Si–O–Si bridge configurations are also found after 1.5 ps. The structure is less distorted than the case of α_2-$SiSO_{0.5}$ due to the smaller degree of oxidation but still on the brink of degradation. Both α_2-$SiSO_{0.5}$ and α-$SiSO_{0.25}$ get degraded even faster at higher temperature of 500 K. The fully oxidized surface of α-SiS with good stability under high temperature indicates the possibility of approaches to synthesize α-SiSO monolayer or few layers by chemical vapor

DOI: 10.1021/acs.jpcc.9b08025
J. Phys. Chem. C 2019, 123, 29986–29993

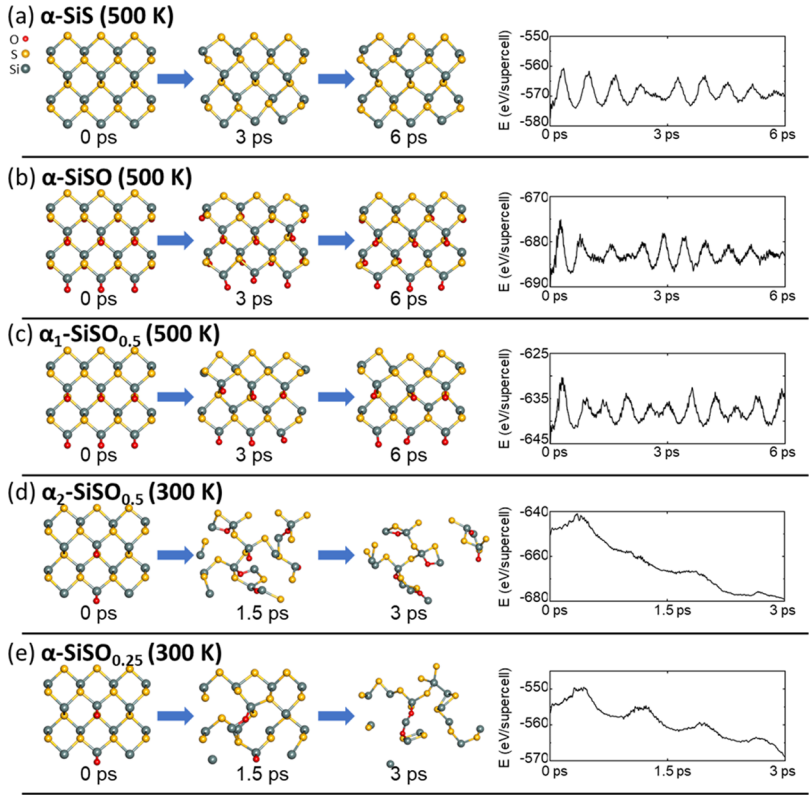

Figure 7. Snap shots of structural changes (left panel) and fluctuations of total potential energy (right panel) during canonical molecular dynamics simulations for (a) α-SiS, (b) α-SiSO, (c) α_1-$SiSO_{0.5}$ monolayers under the temperature 500 K, and (d) α_2-$SiSO_{0.5}$, (e) α-$SiSO_{0.25}$ monolayers under the temperature 300 K.

deposition with a controllable ratio of oxygen and an appropriate substrate, and the possibility of application for α-SiSO as the protecting layer in experimental preparation of the pristine 2D SiS structure.

4. CONCLUSIONS

In summary, we have investigated isolated oxygen impurities of 2D α-SiS, β-SiS, *Pma*2-SiS, and silicene sulfide structures by ab initio DFT calculations. Binding energies of possible geometries for the oxygen impurities in the four SiS monolayers were calculated and the most stable configurations were determined. All the four 2D SiS structures are found more prone to oxidation than black phosphorene, due to the lower electronegativity of Si atoms and inclination to transfer electrons to O atoms. The 2D stoichiometric SiSO structures corresponding to the most stable oxidation configurations of the four pristine SiS structures have been predicted. Vibrational phonon spectra calculations show that only 2D α-SiSO among the four stoichiometric SiSO structures is dynamically stable. Electronic structure calculations indicate that α-SiSO monolayer is semiconducting with a direct band gap of 2.28 eV at PBE level and 3.73 eV at HSE06 level. The value of band gap can be tuned from 1.60 to 2.73 eV in PBE and from 2.90 to 4.16 eV in HSE06, within 10% uniaxial in-layer strain. A direct-to-indirect gap transition can happen under compressive strain along both directions. The value of band gap for 2D α-$SiSO_x$ ($0 \le x \le 1$) structures was found dramatically increasing with the value of x when oxidized on both sides while keeping nearly unchanged when oxidized on one single side. Our AIMD simulations show that α-SiSO and α_1-$SiSO_{0.5}$ structures with all Si atoms attached by O atoms on one or both oxidized surfaces are as stable as α-SiS under high temperature at 500 K. While α_2-$SiSO_{0.5}$ and α-$SiSO_{0.25}$ structures with bare Si atoms on the oxidized surfaces have poorer thermodynamic stability and are easy to get degraded even at room temperature of 300 K, due to the attractive interaction between O atoms and the neighboring exposed Si atoms. The fully oxidized surface of α-SiS with good stability at high temperature could be used as the protecting layer for the pristine 2D structure in application.

■ ASSOCIATED CONTENT

Supporting Information

The Supporting Information is available free of charge at https://pubs.acs.org/doi/10.1021/acs.jpcc.9b08025.

SiSO18-SI.pdf: Additional information for interaction between O atoms absorbed on α-SiS, detailed PDOS for α-SiSO, electronic structure of strained α-SiSO and α-$SiSO_x$ ($x < 1$), interlayer interaction and band gap for multilayer α-SiSO, phonon spectra based on LDA functional, electronic properties for unstable SiSO monolayers, GW band structure of α-SiSO, structural information for the predicted structures (PDF)

■ AUTHOR INFORMATION

Corresponding Author

*E-mail: guanjie@seu.edu.cn. Phone: +86-025-52090600-8306.

ORCID

Shuai Dong: 0000-0002-6910-6319

Jie Guan: 0000-0003-2620-2279

DOI: 10.1021/acs.jpcc.9b08025
J. Phys. Chem. C 2019, 123, 29986−29993

Notes

The authors declare no competing financial interest.

■ ACKNOWLEDGMENTS

This study was supported by National Natural Science Foundation of China (NSFC) under grant nos 61704110, 11674055, and 11834002, by Fundamental Research Funds for the Central Universities, by Shuangchuang Doctor Program of Jiangsu Province, and by Zhongying Young Scholar Program of Southeast University.

■ REFERENCES

(1) Novoselov, K. S.; Geim, A. K.; Morozov, S. V.; Jiang, D.; Zhang, Y.; Dubonos, S. V.; Grigorieva, I. V.; Firsov, A. A. Electric Field Effect in Atomically Thin Carbon Films. *Science* **2004**, *306*, 666−669.

(2) Li, L.; Yu, Y.; Ye, G. J.; Ge, Q.; Ou, X.; Wu, H.; Feng, D.; Chen, X. H.; Zhang, Y. Black Phosphorus Field-Effect Transistors. *Nat. Nanotechnol.* **2014**, *9*, 372−377.

(3) Liu, H.; Neal, A. T.; Zhu, Z.; Luo, Z.; Xu, X.; Tománek, D.; Ye, P. D. Phosphorene: an Unexplored 2D Semiconductor with a High Hole Mobility. *ACS Nano* **2014**, *8*, 4033−4041.

(4) Koenig, S. P.; Doganov, R. A.; Schmidt, H.; Castro Neto, A. H.; Özyilmaz, B. Electric Field Effect in Ultrathin Black Phosphorus. *Appl. Phys. Lett.* **2014**, *104*, 103106.

(5) Low, T.; Engel, M.; Steiner, M.; Avouris, P. Origin of Photoresponse in Black Phosphorus Phototransistors. *Phys. Rev. B: Condens. Matter Mater. Phys.* **2014**, *90*, No. 081408(R).

(6) Zhu, Z.; Guan, J.; Liu, D.; Tománek, D. Designing Isoelectronic Counterparts to Layered Group V Semiconductors. *ACS Nano* **2015**, *9*, 8284−8290.

(7) Yang, J.-H.; Zhang, Y.; Yin, W.-J.; Gong, X. G.; Yakobson, B. I.; Wei, S.-H. Two-Dimensional SiS Layers With Promising Electronic and Optoelectronic Properties: Theoretical Prediction. *Nano Lett.* **2016**, *16*, 1110−1117.

(8) Gomes, L. C.; Carvalho, A. Phosphorene Analogues: Isoelectronic Two-Dimensional Group-IV Monochalcogenides with Orthorhombic Structure. *Phys. Rev. B: Condens. Matter Mater. Phys.* **2015**, *92*, 085406.

(9) Kamal, C.; Chakrabarti, A.; Ezawa, M. Direct Band Gaps in Group IV-VI Monolayer Materials: Binary Counterparts of Phosphorene. *Phys. Rev. B* **2016**, *93*, 125428.

(10) Fei, R.; Li, W.; Li, J.; Yang, L. Giant Piezoelectricity of Monolayer Group IV Monochalcogenides: SnSe, SnS, GeSe, and GeS. *Appl. Phys. Lett.* **2015**, *107*, 173104.

(11) Gomes, L. C.; Carvalho, A.; Castro Neto, A. H. Enhanced Piezoelectricity and Modified Dielectric Screening of Two-Dimensional Group-IV Monochalcogenides. *Phys. Rev. B: Condens. Matter Mater. Phys.* **2015**, *92*, 214103.

(12) Zhang, K.; Deng, K.; Li, J.; Zhang, H.; Yao, W.; Denlinger, J.; Wu, Y.; Duan, W.; Zhou, S. Widely Tunable Band Gap in a Multivalley Semiconductor SnSe by Potassium Doping. *Phys. Rev. Mater.* **2018**, *2*, 054603.

(13) Fei, R.; Kang, W.; Yang, L. Ferroelectricity and Phase Transitions in Monolayer Group-IV Monochalcogenides. *Phys. Rev. Lett.* **2016**, *117*, 097601.

(14) Chang, K.; Liu, J.; Lin, H.; Wang, N.; Zhao, K.; Zhang, A.; Jin, F.; Zhong, Y.; Hu, X.; Duan, W.; Zhang, Q.; Fu, L.; Xue, Q.-K.; Chen, X.; Ji, S.-H. Discovery of Robust in-Plane Ferroelectricity in Atomic-Thick SnTe. *Science* **2016**, *353*, 274−278.

(15) Liu, K.; Lu, J.; Picozzi, S.; Bellaiche, L.; Xiang, H. Intrinsic Origin of Enhancement of Ferroelectricity in SnTe Ultrathin Films. *Phys. Rev. Lett.* **2018**, *121*, 027601.

(16) Barraza-Lopez, S.; Kaloni, T. P.; Poudel, S. P.; Kumar, P. Tuning the Ferroelectric-to-Paraelectric Transition Temperature and Dipole Orientation of Group-IV Monochalcogenide Monolayers. *Phys. Rev. B* **2018**, *97*, 024110.

(17) Zhao, L.-D.; Lo, S.-H.; Zhang, Y.; Sun, H.; Tan, G.; Uher, C.; Wolverton, C.; Dravid, V. P.; Kanatzidis, M. G. Ultralow Thermal Conductivity and High Thermoelectric Figure of Merit in SnSe Crystals. *Nature* **2014**, *508*, 373.

(18) Shafique, A.; Shin, Y.-H. Thermoelectric and Phonon Transport Properties of Two-Dimensional IV−VI Compounds. *Sci. Rep.* **2017**, *7*, 506.

(19) Jiang, H. R.; Zhao, T. S.; Liu, M.; Wu, M. C.; Yan, X. H. Two-Dimensional SiS as a Potential Anode Material for Lithium-Based Batteries: A First-Principles Study. *J. Power Sources* **2016**, *331*, 391−399.

(20) Haleoot, R.; Paillard, C.; Kaloni, T. P.; Mehboudi, M.; Xu, B.; Bellaiche, L.; Barraza-Lopez, S. Photostrictive Two-Dimensional Materials in the Monochalcogenide Family. *Phys. Rev. Lett.* **2017**, *118*, 227401.

(21) Xu, L.; Yang, M.; Wang, S. J.; Feng, Y. P. Electronic and Optical Properties of the Monolayer Group-IV Monochalcogenides MX (M=Ge,Sn; X=S,Se,Te). *Phys. Rev. B* **2017**, *95*, 235434.

(22) Rangel, T.; Fregoso, B. M.; Mendoza, B. S.; Morimoto, T.; Moore, J. E.; Neaton, J. B. Large Bulk Photovoltaic Effect and Spontaneous Polarization of Single-Layer Monochalcogenides. *Phys. Rev. Lett.* **2017**, *119*, 067402.

(23) Xue, D.-J.; Liu, S.-C.; Dai, C.-M.; Chen, S.; He, C.; Zhao, L.; Hu, J.-S.; Wan, L.-J. GeSe Thin-Film Solar Cells Fabricated by Self-Regulated Rapid Thermal Sublimation. *J. Am. Chem. Soc.* **2017**, *139*, 958−965.

(24) Zhao, P.; Yang, H.; Li, J.; Jin, H.; Wei, W.; Yu, L.; Huang, B.; Dai, Y. Design of New Photovoltaic Systems Based on Two-Dimensional Group-IV Monochalcogenides for High Performance Solar Cells. *J. Mater. Chem. A* **2017**, *5*, 24145−24152.

(25) Wood, J. D.; Wells, S. A.; Jariwala, D.; Chen, K.-S.; Cho, E.; Sangwan, V. K.; Liu, X.; Lauhon, L. J.; Marks, T. J.; Hersam, M. C. Effective Passivation of Exfoliated Black Phosphorus Transistors Against Ambient Degradation. *Nano Lett.* **2014**, *14*, 6964−6970.

(26) Favron, A.; Gaufrès, E.; Fossard, F.; Phaneuf-L'Heureux, A.-L.; Tang, N. Y.-W.; Lévesque, P. L.; Loiseau, A.; Leonelli, R.; Francoeur, S.; Martel, R. Photooxidation and Quantum Confinement Effects in Exfoliated Black Phosphorus. *Nat. Mater.* **2015**, *14*, 826.

(27) Ziletti, A.; Carvalho, A.; Campbell, D. K.; Coker, D. F.; Castro Neto, A. H. Oxygen Defects in Phosphorene. *Phys. Rev. Lett.* **2015**, *114*, 046801.

(28) Zhou, Q.; Chen, Q.; Tong, Y.; Wang, J. Light-Induced Ambient Degradation of Few-Layer Black Phosphorus: Mechanism and Protection. *Angew. Chem., Int. Ed.* **2016**, *128*, 11609−11613.

(29) Gomes, L. C.; Carvalho, A.; Castro Neto, A. H. Vacancies and Oxidation of Two-Dimensional Group-IV Monochalcogenides. *Phys. Rev. B* **2016**, *94*, 054103.

(30) Eda, G.; Chhowalla, M. Chemically Derived Graphene Oxide: Towards Large-Area Thin-Film Electronics and Optoelectronics. *Adv. Mater.* **2010**, *22*, 2392−2415.

(31) Robinson, J. T.; Zalalutdinov, M.; Baldwin, J. W.; Snow, E. S.; Wei, Z.; Sheehan, P.; Houston, B. H. Wafer-Scale Reduced Graphene Oxide Films for Nanomechanical Devices. *Nano Lett.* **2008**, *8*, 3441−3445.

(32) Robinson, J. T.; Perkins, F. K.; Snow, E. S.; Wei, Z.; Sheehan, P. E. Reduced Graphene Oxide Molecular Sensors. *Nano Lett.* **2008**, *8*, 3137−3140.

(33) Mortazavi, B.; Shahrokhi, M.; Hussain, T.; Zhuang, X.; Rabczuk, T. Theoretical Realization of Two-Dimensional M3(C6X6)-2 (M=Co, Cr, Cu, Fe, Mn, Ni, Pd, Rh and X=O, S, Se) Metal−Organic Frameworks. *Appl. Mater. Today* **2019**, *15*, 405−415.

(34) Mortazavi, B.; Shahrokhi, M.; Madjet, M. E.; Hussain, T.; Zhuang, X.; Rabczuk, T. N-, B-, P-, Al-, As-, and Ga-Graphdiyne/Graphyne Lattices: First-Principles Investigation of Mechanical, Optical and Electronic Properties. *J. Mater. Chem. C* **2019**, *7*, 3025−3036.

(35) Wang, G.; Pandey, R.; Karna, S. P. Phosphorene Oxide: Stability and Electronic Properties of a Novel Two-Dimensional Material. *Nanoscale* **2015**, *7*, 524−531.

(36) Ziletti, A.; Carvalho, A.; Trevisanutto, P. E.; Campbell, D. K.; Coker, D. F.; Castro Neto, A. H. Phosphorene Oxides: Bandgap

DOI: 10.1021/acs.jpcc.9b08025
J. Phys. Chem. C 2019, 123, 29986−29993

Engineering of Phosphorene by Oxidation. *Phys. Rev. B: Condens. Matter Mater. Phys.* **2015**, *91*, 085407.
(37) Kresse, G.; Furthmüller, J. Efficient Iterative Schemes for Ab Initio Total-Energy Calculations Using a Plane-Wave Basis Set. *Phys. Rev. B: Condens. Matter Mater. Phys.* **1996**, *54*, 11169−11186.
(38) Kresse, G.; Hafner, J. Ab Initio Molecular Dynamics for Liquid Metals. *Phys. Rev. B: Condens. Matter Mater. Phys.* **1993**, *47*, 558−561.
(39) Kresse, G.; Hafner, J. Ab Initio Molecular-Dynamics Simulation of the Liquid-Metal-Amorphous-Semiconductor Transition in Germanium. *Phys. Rev. B: Condens. Matter Mater. Phys.* **1994**, *49*, 14251−14269.
(40) Monkhorst, H. J.; Pack, J. D. Special Points for Brillouin-Zone Integrations. *Phys. Rev. B: Solid State* **1976**, *13*, 5188−5192.
(41) Kresse, G.; Joubert, D. From Ultrasoft Pseudopotentials to the Projector Augmented-Wave Method. *Phys. Rev. B: Condens. Matter Mater. Phys.* **1999**, *59*, 1758−1775.
(42) Perdew, J. P.; Burke, K.; Ernzerhof, M. Generalized Gradient Approximation Made Simple. *Phys. Rev. Lett.* **1996**, *77*, 3865−3868.
(43) Hestenes, M. R.; Stiefel, E. Methods of Conjugate Gradients for Solving Linear Systems. *J. Res. Natl. Bur. Stand.* **1952**, *49*, 409−436.
(44) Togo, A.; Tanaka, I. First Principles Phonon Calculations in Materials Science. *Scr. Mater.* **2015**, *108*, 1−5.
(45) Heyd, J.; Scuseria, G. E.; Ernzerhof, M. Erratum: "Hybrid Functionals Based on a Screened Coulomb Potential" [J. Chem. Phys. 118, 8207 (2003)]. *J. Chem. Phys.* **2006**, *124*, 219906.
(46) Hedin, L. New Method for Calculating the One-Particle Green's Function with Application to the Electron-Gas Problem. *Phys. Rev.* **1965**, *139*, A796−A823.
(47) Shishkin, M.; Kresse, G. Self-Consistent GW Calculations for Semiconductors and Insulators. *Phys. Rev. B: Condens. Matter Mater. Phys.* **2007**, *75*, 235102.
(48) Grimme, S. Semiempirical GGA-Type Density Functional Constructed with a Long-Range Dispersion Correction. *J. Comput. Chem.* **2006**, *27*, 1787−1799.
(49) Zhu, Z.; Tománek, D. Semiconducting Layered Blue Phosphorus: A Computational Study. *Phys. Rev. Lett.* **2014**, *112*, 176802.
(50) Guan, J.; Zhu, Z.; Tománek, D. Phase Coexistence and Metal-Insulator Transition in Few-Layer Phosphorene: A Computational Study. *Phys. Rev. Lett.* **2014**, *113*, 046804.
(51) Liu, D.; Every, A. G.; Tománek, D. Continuum Approach for Long-Wavelength Acoustic Phonons in Quasi-Two-Dimensional Structures. *Phys. Rev. B* **2016**, *94*, 165432.
(52) Yu, W.; Niu, C.-Y.; Zhu, Z.; Wang, X.; Zhang, W.-B. Atomically Thin Binary V−V Compound Semiconductor: a First-Principles Study. *J. Mater. Chem. C* **2016**, *4*, 6581−6587.
(53) Grumet, M.; Liu, P.; Kaltak, M.; Klimeš, J.; Kresse, G. Beyond the Quasiparticle Approximation: Fully Self-Consistent GW Calculations. *Phys. Rev. B* **2018**, *98*, 155143.
(54) Wei, Q.; Peng, X. Superior Mechanical Flexibility of Phosphorene and Few-Layer Black Phosphorus. *Appl. Phys. Lett.* **2014**, *104*, 251915.
(55) Shulenberger, L.; Baczewski, A. D.; Zhu, Z.; Guan, J.; Tomanek, D. The Nature of the Interlayer Interaction in Bulk and Few-Layer Phosphorus. *Nano Lett.* **2015**, *15*, 8170−8175.

DOI: 10.1021/acs.jpcc.9b08025
J. Phys. Chem. C 2019, 123, 29986−29993